ACS APPLIED MATERIALS & INTERFACES

Research Article

Cite This: ACS Appl. Mater. Interfaces 2019, 11, 21904−21914

www.acsami.org

Superhydrophobic Electrically Conductive Paper for Ultrasensitive Strain Sensor with Excellent Anticorrosion and Self-Cleaning Property

Qianming Li,[†] Hu Liu,[*,†,‡] Shuaidi Zhang,[†] Dianbo Zhang,[†] Xianhu Liu,[†] Yuxin He,[§] Liwei Mi,[∥] Jiaoxia Zhang,[‡] Chuntai Liu,[†,⊥] Changyu Shen,[†] and Zhanhu Guo[‡]

[†]Key Laboratory of Materials Processing and Mold (Zhengzhou University), Ministry of Education; National Engineering Research Center for Advanced Polymer Processing Technology, Zhengzhou University, Zhengzhou, Henan 450002, China

[‡]Integrated Composites Laboratory (ICL), Department of Chemical & Biomolecular Engineering, University of Tennessee, Knoxville, Tennessee 37996, United States

[§]College of Chemical Engineering and Pharmaceutics, Henan University of Science and Technology, Luoyang, Henan 471023, China

[∥]Center for Advanced Materials Research, Zhongyuan University of Technology, Zhengzhou, Henan 450007, China

[⊥]Technology Development Center for Polymer Processing Engineering, Guangdong Colleges and Universities, Guangdong Industry Technical College, Guangzhou, Guangdong 510641, China

Supporting Information

ABSTRACT: Recently, a paper-based (PB) strain sensor has turned out to be an ideal substitute for the polymer-based one because of the merits of renewability, biodegradability, and low cost. However, the hygroexpansion and degradation of the paper after absorbing water are the great challenges for the practical applications of the PB strain sensor. Herein, the superhydrophobic electrically conductive paper was fabricated by simply dip-coating the printing paper into the carbon black (CB)/carbon nanotube (CNT)/methyl cellulose suspension and hydrophobic fumed silica (Hf-SiO_2) suspension successively to settle the problem. Because of the existence of ultrasensitive microcrack structures in the electrically conductive CB/CNT layer, the sensor was capable of detecting an ultralow strain as low as 0.1%. During the tension strain range of 0−0.7%, the sensor exhibited a gauge factor of 7.5, almost 3 times higher than that of the conventional metallic-based sensors. In addition, the sensor displayed frequency-independent and excellent durability and reproductivity over 1000 tension cycles. Meanwhile, the superhydrophobic Hf-SiO_2 layer with a micro−nano structure and low surface energy endowed the sensor with outstanding waterproof and self-cleaning properties, as well as great sustainability toward cyclic strain and harsh corrosive environment. Finally, the PB strain sensor could effectively monitor human bodily motions such as finger/elbow joint/throat movement and pulse in real time, especially for the wet or rainy conditions. All these pave way for the fabrication of a high-performance PB strain sensor.

KEYWORDS: *paper, ultrasensitive, superhydrophobic, strain sensor, human bodily motion*

1. INTRODUCTION

With the rapid development of electronic industry, flexible electronic devices (such as strain sensors, supercapacitors, nanogenerators, etc.) are urgently required in many fields, including soft robotic systems,[1,2] electronic skins,[3−5] human health monitoring,[6−11] flexible displays,[12] man−machine interface systems,[13−15] and so forth. Among them, the flexible resistive-type strain sensor, which converts mechanical deformation into a resistance variation signal, has received great attention, and lots of investigations based on the flexible polymer matrix have been widely conducted to acquire new high-performance products.[16−21] However, most polymers are difficult to be recycled or degraded,[22,23] which will undoubtedly bring plenty of electronic wastes and thus cause enormous environmental problems in the near future. To solve this problem, paper with the merits of renewability,[24,25] biodegradability,[26] and low cost[27,28] turns out to be an ideal substrate to fabricate green degradable strain sensors in some recently published papers.

Paper-based (PB) strain sensors are usually fabricated by simply dip-coating the paper into electrically conductive filler suspensions.[27,29−31] In general, carbonaceous fillers [e.g., zero-dimensional carbon black (CB), one-dimensional carbon nanotube (CNT), and two-dimensional graphene],[10,32−39]

Received: February 23, 2019
Accepted: May 24, 2019
Published: May 24, 2019

DOI: 10.1021/acsami.9b03421
ACS Appl. Mater. Interfaces 2019, 11, 21904−21914

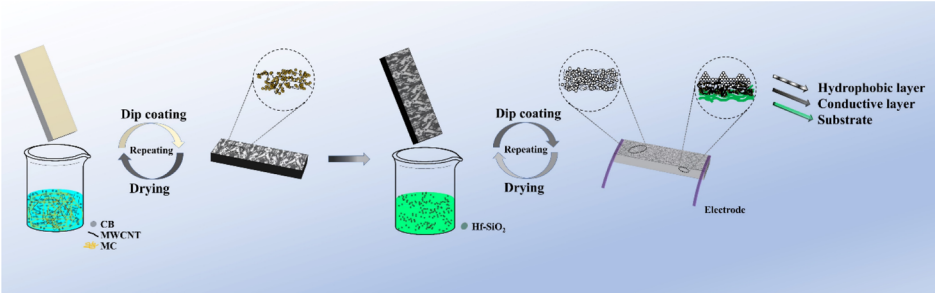

Figure 1. Schematic illustration for the preparation of superhydrophobic electrically conductive paper.

metallic fillers,[40,41] and hybrid fillers[42−47] are ideal electrically conductive fillers. To lower the manufacturing cost, low-cost CB is usually adopted. However, CB particles are prone to aggregate in its suspension because of the strong van der Waals force,[48] leading to the inhomogeneous distribution of the electrically conductive filler and unstable sensing performance. Recently, it is proved that the application of hybrid electrically conductive fillers could effectively enhance the dispersity of fillers based on the synergistic effect between them, which will be beneficial for the reduction of the percolation threshold and the improvement of the stability of sensing performance arising from the simple and stable hybrid conductive network.[49−55] For instance, Liu et al. successfully prepared thermoplastic polyurethane (TPU)/CNT/graphene nanocomposites, and a homogeneous dispersion of the hybrid filler was obtained through the synergistic effect between CNT and graphene.[44] Here, entangled CNTs were separated and connected by a single-layer graphene, achieving a stable conductive network and excellent strain sensing behavior. Hence, the usage of a secondary filler with CB can be more effective and suitable for a large-scale production.

Meanwhile, the practical application requirements for the flexible strain sensors in wearable electronics also raise new expectations with other properties, such as waterproof, corrosion-resistant (e.g., human sweat, soapy water, and acid rain), and self-cleaning characteristics.[56−58] All these appear to be more important for PB strain sensors because of the hygroexpansion and degradation of paper after absorbing water, causing the invalidation of the sensor.[27] Therefore, it is of significant value to prepare PB strain sensors with superhydrophobicity. Recently, superhydrophobic polymer-based strain sensors, including modified silver nanoparticles/polystyrene-*b*-poly(ethylene-*co*-butylene)-*b*-polystyrene (SEBS)/natural rubber,[59] CNT/SEBS,[20] perfluoro silane/graphene/TPU,[60] and so forth, have been successively fabricated, and the influence of wet condition on the sensing performance has been effectively eliminated. For example, Li et al. prepared electrically conductive CNT/SEBS composites with a sustainable superhydrophobicity arising from the micrometer-sized pit-like rough surface, and the composites exhibited a stable sensing performance over a wide stain range when used as strain sensors.[20] However, superhydrophobic PB strain sensors have rarely been reported.

In this study, superhydrophobic electrically conductive paper was successfully fabricated by dip-coating the printing paper into the CB/CNT/methyl cellulose (MC) suspension and hydrophobic fumed silica (Hf-SiO_2) suspension successively. Here, CNT was used as the secondary filler to improve the dispersity of CB and construct a more stable conductive network. In addition, MC was used as a dispersant and binder to improve the dispersity of fillers and the adhesion between the electrically conductive filler and the paper. Then, the electrical property and water contact angle (WCA) of the paper were investigated, and scanning electron microscopy (SEM) was conducted to study the microstructure of the electrically conductive CB/CNT layer and superhydrophobic Hf-SiO_2 layer. As for the feasibility of the paper for strain sensor, the strain sensing behaviors under different strain frequencies and cyclic strain were investigated systematically. Besides, the self-cleaning property, the anticorrosion performance, and the stability of the superhydrophobicity were also evaluated. Finally, the PB strain sensor was applied to detect human bodily motions to demonstrate its potential application for wearable electronic devices.

2. EXPERIMENTAL SECTION

2.1. Materials. CB (VXC-72) with a particle diameter of 30 nm was purchased from Cabot Co. Ltd., USA. CNTs with the −COOH content of 1.23 wt % were bought from Chengdu Organic Chemicals Co. Ltd., Chinese Academy of Sciences. According to the producer, the diameter and length of CNTs were 25 nm and 20 μm, respectively. Hf-SiO_2 with a specific surface area of 110 m^2/g, diameter of 16 nm, and carbon content of 0.9 wt % was obtained from Evonik Industries Co. Ltd., Germany. MC with a molecular weight of 40 000−180 000 $g{\cdot}mol^{-1}$ was bought from Tianjin Damao Chemical Reagent Factory, Tianjin, China. Anhydrous ethanol was purchased from Tianjin Fuyu Fine Chemical Co., Ltd., China. All the materials and reagents were used as received.

2.2. Preparation of Superhydrophobic Electrically Conductive Paper. Superhydrophobic electrically conductive paper was prepared by successively dipping the printing paper into the CB/CNT/MC suspension and Hf-SiO_2 suspension, as illustrated in Figure 1. For the preparation of CB/CNT/MC suspension, CB, CNT, and MC were first added into the mixture of anhydrous ethanol and deionized (DI) water with a volume ratio of 1:1 followed by ultrasonication treatment (200W, DS-1000Y, Dusi Instrument Co. Ltd., Shanghai) for 20 min. Here, the effects of MC and conductive filler loading on the stability of the suspension were systematically studied to obtain a suitable suspension for the dip-coating technique. Besides, Hf-SiO_2 suspension (0.1 g/mL) was obtained by the ultrasonic dispersion of Hf-SiO_2 particles into anhydrous ethanol for 10 min to obtain a stable suspension. Next, the printing paper strip with a length of 50 mm and width of 12 mm was first dipped into the CB/CNT/MC suspension and then dried at 50 °C for 1 h repeatedly, achieving an electrically conductive CB/CNT-coated paper. Finally, the CB/CNT-coated paper was dipped into the Hf-SiO_2 suspension and dried at 50 °C repeatedly to obtain the superhydrophobic electrically conductive Hf-SiO_2/CB/CNT-coated paper.

2.3. Characterization. The morphology and microstructure of the paper were observed using SEM (JEOL JSM-7500F) at an accelerating voltage of 5 kV after spray-coating of gold. Fourier transform infrared (FT-IR) spectra in the range of 500−4000 cm^{-1} were recorded on a Nicolet Nexus 870 instrument using the attenuated total reflectance technique. Raman spectra in the range

DOI: 10.1021/acsami.9b03421
ACS Appl. Mater. Interfaces 2019, 11, 21904−21914

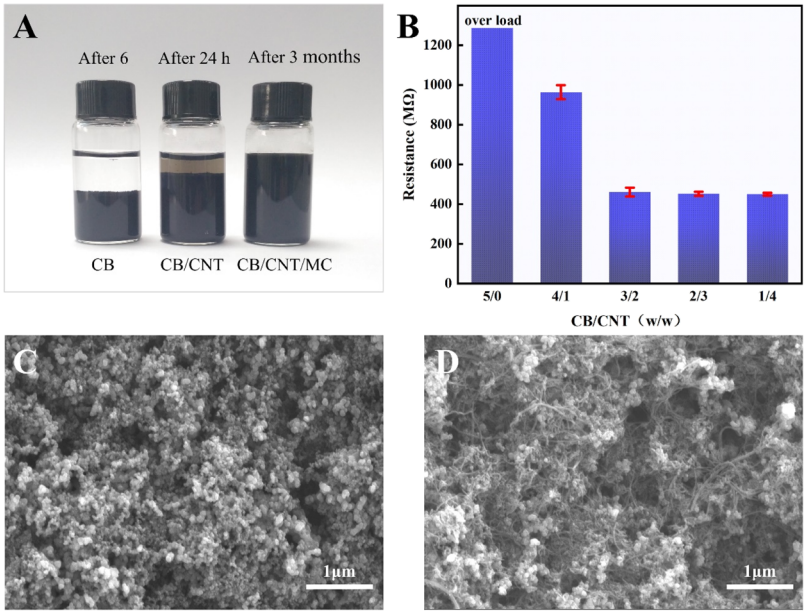

Figure 2. (A) Digital photos showing the settlement state of different suspensions after sonication; (B) relationship between the mass ratio of the hybrid filler and the resistance of CB/CNT-coated paper after coating one time; SEM images of the surface of (C) CB and (D) CB/CNT-coated paper.

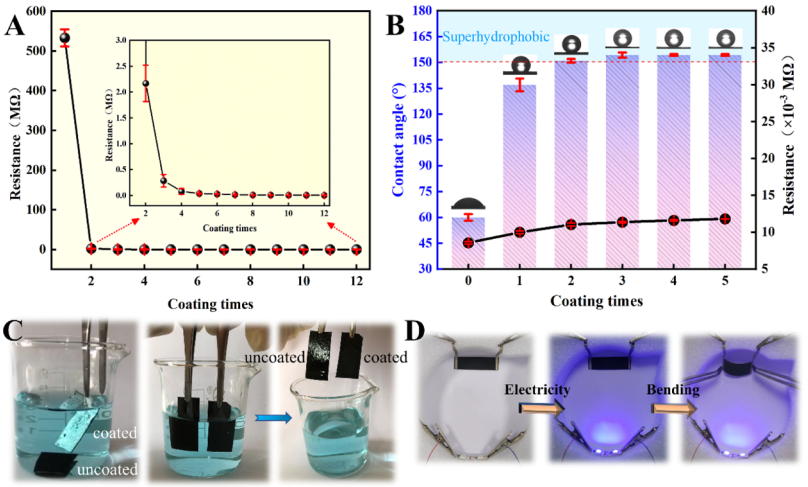

Figure 3. (A) Resistance of CB/CNT (3/2)-coated paper as a function of coating times; (B) WCA and resistance of Hf-SiO_2/CB/CNT-coated paper as a function of coating times. Insets: Representative optical photographs showing the water droplets (≈5 μL) on the coated papers. (C) Pictures of Hf-SiO_2-coated and uncoated electrically conductive paper immersed/removed in water and (D) pictures of an LED circuit connected with the Hf-SiO_2/CB/CNT-coated paper (an unplugged LED was placed in the left as a reference).

of 500−3500 cm^{-1} were obtained by utilizing confocal Raman spectroscopy (HORIBA LabRAM HR Evolution) at room temperature. WCA was measured by using an optical contact angle meter (SL200KS USA KINO Industry Co., Ltd.) at room temperature. During the test, 5 μL of water was dropped onto the surface of the paper, and WCA was determined by averaging the measurements of at least five different positions.

Electrodes were stickled onto the same side of both ends of the superhydrophobic electrically conductive paper using silver paste to fabricate the PB strain sensor. The resistance of the sensor was measured using a digital multimeter (Tektronix DMM4050), and at least five strips were tested for each sample. For the cyclic strain sensing test, the digital multimeter (Tektronix DMM4050) was coupled with a universal tensile testing machine (Shimadzu, Japan), and the variation of resistance upon loading was recorded online (Figure S1).

The current−voltage (I−V) curves of the sensor were measured via linear sweep voltammetry using an RST5000 electrochemical workstation (Suzhou Risetest Electronic Co., Ltd., China). The voltage range was typically set between −5 and +5 V.

3. RESULTS AND DISCUSSION

3.1. Preparation of CB/CNT/MC Hybrid Suspension.

Generally, a long-term stable and uniform aqueous suspension of the conductive filler is crucial for the dip-coating technique. As shown in Figure 2A, the CB aqueous suspension exhibited a rapid settlement in 6 h after the ultrasonication treatment because of the strong van der Waals forces between the CB particles. With the addition of CNTs, the aggregation of CB particles was effectively solved with the assistance of the synergistic effect between different dimensional conductive fillers (Figure S2). However, the suspension of hybrid fillers

DOI: 10.1021/acsami.9b03421
ACS Appl. Mater. Interfaces 2019, 11, 21904−21914

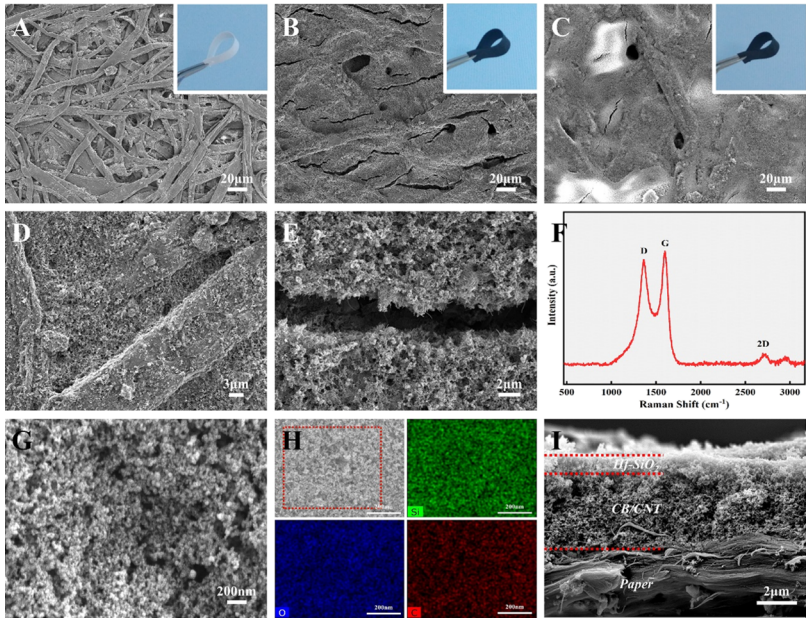

Figure 4. SEM images of the surface of (A) original paper, (B) CB/CNT-coated paper, and (C) Hf-SiO_2/CB/CNT-coated paper. Insets are their corresponding physical photographs; (D,E) high-magnification image of (B) showing the rough cellulose fibers and the microcrack structure, respectively; (F) Raman spectrum of the surface of the CB/CNT-coated paper; (G) high-magnification image of (C) showing the microstructure of the Hf-SiO_2 layer; (H) elemental mapping of the surface of the Hf-SiO_2/CB/CNT-coated paper; (I) SEM image of the cross section of the Hf-SiO_2/CB/MWNT-coated paper.

displayed the aggregation of conductive fillers again after 48 h, indicating that the addition of a secondary filler also could not satisfy the actual need. Then, it is surprising to observe that MC used as a dispersant could effectively improve the stability of the hybrid filler suspension for at least 3 months. Hybrid fillers (0.1 g) and 0.05 g MC dispersed in 20 mL of mixed solvent were good for a stable suspension (Table S1). Higher MC or hybrid filler loading would generate a gel, which is not suitable for the dip-coating technique.

After dip-coating one time, the influence of the mass ratio of CB/CNT on the resistance of the CB/CNT-coated paper was studied to achieve a proper mass ratio. It can be seen clearly in Figure 2B that the resistance of the paper decreased significantly with increasing CNT loading, indicating the construction of more perfect conductive networks with the assistance of CNTs. Then, the resistance of the paper tended to be constant when the mass ratio was reduced to 3:2. Furthermore, the microstructure of the conductive network distributed on the surface of the paper was also characterized, as illustrated in Figure 2C,D. For CB-coated paper, the existence of isolated CB aggregation was detrimental to the construction of an effective conductive network, leading to a higher resistance. As for the CB/CNT-coated paper, CNT acted as a "bridge" to connect the gap between individual CB clusters, favoring the formation of effective conductive paths. All these indicated that the addition of CNT could effectively reduce the resistance of the CB/CNT-coated paper. Therefore, the mass ratio of CB/CNT was identified as 3:2 for the following investigation.

3.2. Properties of the Superhydrophobic Electrically Conductive Paper. As shown in Figure 3A, the relationship between the resistance of the CB/CNT-coated paper and the coating times was studied. It can be seen clearly that the resistance decreased rapidly from 533 MΩ after coating one time to 2.2 MΩ after coating two times. Then, it decreased slightly in the successive coating cycles and tended to be constant from the eighth time, indicating that the conductive network reached a stable state. Next, the CB/CNT-coated paper after coating eight times was further coated with Hf-SiO_2 to fabricate Hf-SiO_2/CB/CNT-coated paper, and the superhydrophobicity of the paper was influenced by the coating times in the Hf-SiO_2 suspension (see Figure 3B). It can be obviously found that WCA sharply increased from 60° for the electrically conductive paper uncoated with Hf-SiO_2 to 136° after coating one time and then further to 154° after coating three times, indicating the transformation of the paper surface from hydrophilic to superhydrophobic. With a further increase of coating times, the WCA remained almost unchanged, indicating that the structure of the superhydrophobic surface tended to be a stable state. Interestingly, when the Hf-SiO_2/CB/CNT-coated paper was immersed into water, it displayed a strong light reflection and remained completely dry after being removed from water compared with the CB/CNT-coated paper (Figure 3C and Video S1). All these indicated that the water drops were in the Cassie−Baxter state on the Hf-SiO_2/CB/CNT-coated paper surface in this work.[61,62] On the other hand, the resistance of the Hf-SiO_2/CB/CNT-coated paper exhibited a slight increase, suggesting that the coating of Hf-SiO_2 had almost no influence on the structure of the CB/CNT conductive network. As a demonstration for its practical application, the Hf-SiO_2/CB/multiwalled CNT (MWNT)-coated paper was integrated with a light-emitting diode (LED) to test its electrical characteristic upon bending, and the brightness of the LED connected with a turn-on voltage of 5 V was reduced when a bending strain was applied, as illustrated in Figure 3D. All these indicated the feasibility of the superhydrophobic electrically conductive coated paper to serve as a waterproof strain sensor to satisfy the practical needs.

3.3. Characterization of the Superhydrophobic Electrically Conductive Paper. From the photographs of

DOI: 10.1021/acsami.9b03421
ACS Appl. Mater. Interfaces 2019, 11, 21904−21914

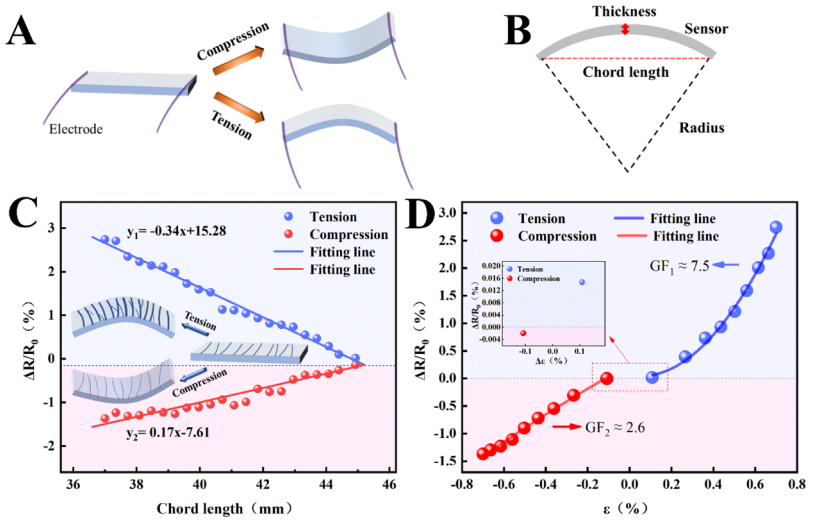

Figure 5. (A) Schematic illustration of compression strain and tension strain; (B) definition of the physical parameters about the PB sensor; relative resistance change as a function of (C) chord length and (D) strain.

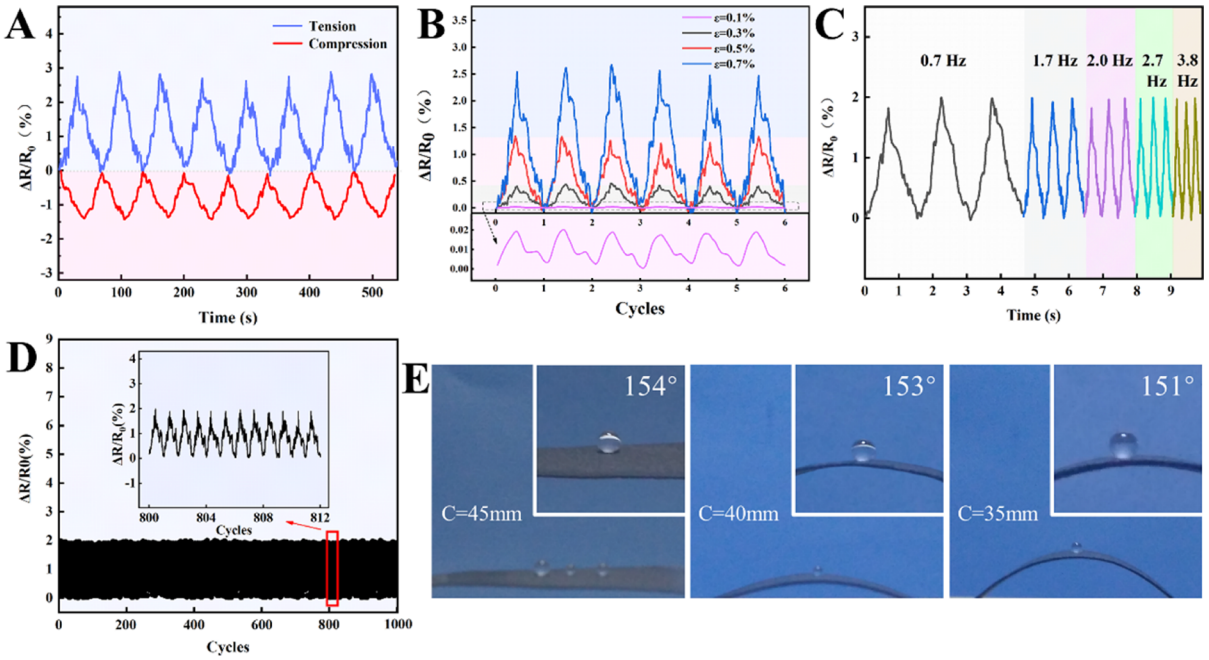

Figure 6. (A) Relative resistance change upon eight compression and tension cycles at a strain of 0.7%; (B) strain sensing behavior of the sensor upon the tension strain of 0.1, 0.3, 0.5, and 0.7%; (C) dynamic sensing performance of the sensor under different tension frequencies at a tension strain of 0.6%; (D) long-term stability of the sensor over 1000 cycles at a tension strain of 0.6%; (E) optical photographs of water droplets (≈5 μL) on the coated paper surfaces with different chord lengths after 1000 tension cycles. Insets: Enlarged photographs showing the WCA.

the insets in Figure 4A,B, it can be observed that the paper substrate turned from white to black and maintained its good flexibility after coating with CB/CNT. As illustrated in Figure 4A,B, the smooth cellulose fibers became rough because of the existence of the CB/CNT hybrid nanoparticles (Figure 4D). Besides, lots of microcracks with an average width of 2 μm existed on the surface (Figure 4E). The formation of microcracks was mainly attributed to the mismatches of the coating and the substrate material in the thermal expansion coefficient and the elastic modulus during the drying process.[27,28] The microcrack structure, which has been widely designed for the preparation of a high-performance strain sensor, holds a great potential to significantly enhance the sensitivity of the sensor based on its propagation and closure upon an external strain.[63−65] Hence, the microcrack here might be helpful for the achievement of highly sensitive strain sensors. Furthermore, Raman spectroscopy was conducted at different points over the CB/CNT coating. The typical scattering peaks observed at 1362, 1712, and 2696 cm^{-1} correspond to the D, G, and 2D bands of CB and CNT (Figure 4F), respectively.[27,66] All these indicated that CB and CNTs are evenly dispersed on the surface of the paper. After further coatingwith Hf-SiO_2, there is almost no change in the color and flexibility of the paper (the inset in Figure 4C). Meanwhile, the paper surface turned to be covered with lots of microscale aggregation of nano-SiO_2, forming a rough surface with a micro−nano structure (Figure 4G). Generally, tailoring the surface microtopography and surface free energy is

DOI: 10.1021/acsami.9b03421
ACS Appl. Mater. Interfaces 2019, 11, 21904−21914

required for a material surface with superhydrophobic properties.[61,67] Here, the micro−nano structure and low surface energy of the Hf-SiO_2 layer would undoubtedly endow the paper with excellent hydrophobicity. Besides, it can be concluded from Figures 4H and S1 that three elements (C, O, and Si) of Hf-SiO_2 are uniformly distributed throughout the whole surface, indicating the good uniformity of Hf-SiO_2 coating. Finally, there was no clear interface between the Hf-SiO_2 layer and the CB/CNT layer (Figure 4I). The strong binding force between them can be ascribed to the existence of hydrogen bonding between the Si−O groups of Hf-SiO_2 and the −OH groups of MC as inferred from the FT-IR spectra (Figure S4). In addition, the swelling of MC during the coating process was also beneficial for the immobilization of Hf-SiO_2 nanoparticles into the CB/CNT layer.

3.4. Strain Sensing Performance of the PB Strain Sensor. As depicted in Figure 5A, compression and tension were defined as the states when the paper was bent forward and backward with fixed electrodes. When the chord length decreased from 45 to 37 mm, the relative resistance variation $\Delta R/R_0$ ($\Delta R = R - R_0$, where R is the resistance in the bending state; R_0 is the initial resistance) of the PB sensor showed a linearly decreasing trend upon compression and a linearly increasing trend upon tension (Figure 5C). To investigate the sensitivity of the PB sensor, gauge factor (GF, $GF = (\Delta R/R_0)/\varepsilon$) was calculated. Here, ε representing the applied strain of the PB sensor upon compression and tension can be calculated to be 0−0.7% according to formulas 1 and 2[17,27,68]

$$\varepsilon = \pm T/2r \tag{1}$$

$$C = 2r\cdot\sin(L/2r) \tag{2}$$

As shown in Figure 5B, T is the thickness of the sensor ($T = T_{paper} + T_{coating} \times 2 = 300\ \mu m + 4.5\ \mu m \times 2 = 309\ \mu m$); L is the length of the PB sensor; C and r are the chord length and curvature radius of the PB sensor upon bending, respectively. Hence, it can be obtained from the fitting results in Figure 5D that the GF of the PB sensor upon compression and tension are 2.6 and 7.5, respectively, showing an ideal sensitivity compared with that of other recent publications.[27,69] As for the different sensing behaviors and sensitivity upon compression and tension, the schematic illustration shown as the inset in Figure 5C can be applied to reveal the sensing mechanism. Some microcracks in the CB/CNT layer would be closed upon compression, causing the increase of the conductive pathway number and the decrease of resistance. Conversely, the external tension strain would induce the opening and propagation of the microcracks, leading to a significant destruction of the conductive network and the increase of resistance. More importantly, the crack propagation would generate more serious influences on the variation of the conductive network than the crack closure.[17,28,68]

Figure 6A displays the cyclic strain sensing behavior of the PB strain sensors upon compression and tension strain (0.7%). During eight cycles, the resistance of the PB sensor recovered to its initial value after removing the external strain, and the response pattern remained unchanged, showing good reproductivity. Meanwhile, the PB sensor also exhibited a stable sensing pattern upon the tension strain of 0.1, 0.3, 0.5, and 0.7% (see Figure 6B), and the resistance variation ratio increased with increasing strain, demonstrating the reliable responses of the sensor to the different applied strains. Notably, an ultralow strain of 0.1% can be accurately and repeatedly detected, which is mainly ascribed to the microcrack structure on the conductive layer. To study the dynamic strain sensing performance of the PB sensor, it was subjected to a cyclic tension strain (such as 0.6%) under different frequencies. As shown in Figure 6C, the PB sensor produced a fast, stable, and highly reproducible response. Besides, the response peak values under different frequencies are all the same, showing the frequency-independent strain sensing behavior. Hence, the PB sensor possessed great potential applications for human bodily motions with different frequencies, including blinking (0.17−0.33 Hz), wrist pulse (1−1.7 Hz), heartbeat (1−2 Hz), and convulsions (1.6−3.3 Hz, patients with epilepsy). Meanwhile, the durability and stability of the PB sensors were also further evaluated through 1000 cycles at a tension strain of 0.6% (Figure 6D). The resistance changed periodically and no obvious fluctuation of the sensing signal was observed. After 1000 tension cycles, the $I-V$ curve of the original PB sensor in Figure S5 displayed a typical linear ohmic behavior, indicating the good stability of the conductive network, which was beneficial for the stable sensing behavior. When the PB strain sensor was applied with an external tension strain, the slope of the $I-V$ curve exhibited a decreased trend, indicating the increase of resistance. After the release of the tension strain, the $I-V$ curve coincided with that of the original one, showing the full restoration of the electrical conductivity. All these verified the good durability, reproductivity, and stability of the PB strain sensor. Finally, the superhydrophobicity of the PB strain sensor was also characterized after 1000 tension cycles. As shown in Figure 6E, when the chord length decreased from 45 to 35 mm, the WCA declined slightly by 3° (154°/45 mm → 153°/40 mm → 151°/35 mm). As a result, the sensor remained superhydrophobic under long-term service, displaying outstanding stability of the superhydrophobicity.

Here, the properties of our superhydrophobic PB strain sensor were compared with the recently published superhydrophobic strain sensors (see Table S2), and the advantages of our strain sensor can be summarized as follows: (1) the low cost (<$0.001), recyclability, and degradability of the PB strain sensor made it to be an ideal alternative to the high-cost and nondegradable polymer-based strain sensor. (2) The PB strain sensor with superhydrophobicity was first fabricated. It could effectively solve the problem of the invalidation of the existing PB strain sensor after absorbing water because of the hygroexpansion and degradation of the paper. Meanwhile, the superhydrophobicity is also helpful for the improvement of stability and service life of all strain sensors in any wet condition during the practical application process. (3) The dip-coating technique was much simpler compared with the complicated techniques, facilitating the large-scale production in practical applications. (4) Compared with other sensitive architectures, the special microcrack architecture in the conductive layer is also an effective method to improve the sensitivity of the sensor upon a small bending strain. What's more, the PB strain sensor in this paper exhibited higher GF compared with other similar ones. All these indicated that our superhydrophobic PB strain sensor possesses broad application prospects.

3.5. Superhydrophobic Performance of the PB Strain Sensor. Considering the influence of harsh outdoor conditions on the superhydrophobicity in practical applications, the anticorrosion property of the PB strain sensor was investigated. First, the PB strain sensor was immersed into a series of aqueous solutions with different pH values (such as

DOI: 10.1021/acsami.9b03421
ACS Appl. Mater. Interfaces 2019, 11, 21904−21914

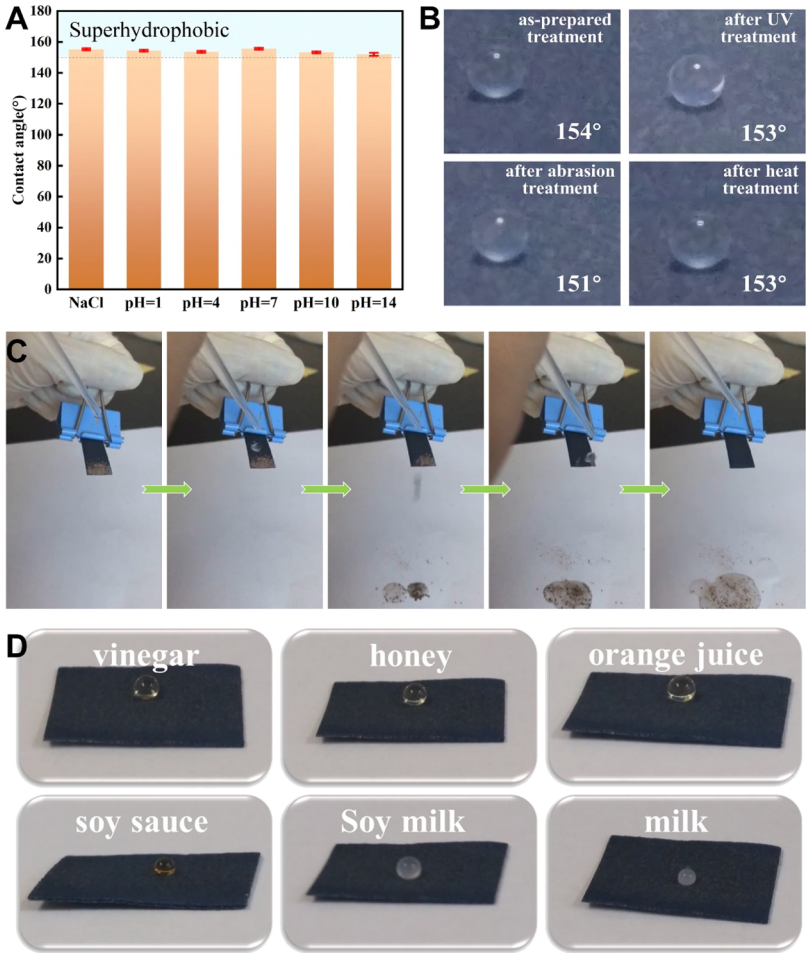

Figure 7. (A) WCAs measured after immersing the paper in aqueous solutions with different pH values for 48 h; (B) optical photographs showing the WCA of water droplets (≈5 μL) on the PB strain sensor as prepared and after different treatments; (C) series of pictures displaying the self-cleaning process of the PB strain sensor; (D) pictures of the droplets of ordinary liquid foods on the surface of the PB strain sensor.

pH = 1, 4, 7, 10, and 14) and sodium chloride solution (3.5 wt %) for 48 h, followed by rinsing with DI water and drying at room temperature. As displayed in Figure 7A, all the measured WCAs were larger than 150°, demonstrating that the pH value of the solution had no influence on the superhydrophobicity. Furthermore, the PB strain sensor was also exposed to ultraviolet radiation (UV-B irradiance, 48 h), water abrasion (water droplets, 20 min), and high temperature treatment (100 °C in an oven, 48 h), and the WCA decreased slightly from 154° to 153°, 151°, and 153°, respectively (Figure 7B), retaining the superhydrophobic property. Hence, the superhydrophobicity of the PB strain sensor could be well-maintained in various harsh environments.

On the other hand, the self-cleaning property, one of the most important applications of superhydrophobicity, was also evaluated. The dust particles attached on the surface of the sensor could be completely taken away immediately by the water droplets during the water-flushing process, revealing the outstanding self-cleaning and extremely water-repellent ability (Figure 7C and Video S2). In addition, wearable sensors may also be contaminated by ordinary liquid foods in daily life. Hence, the self-cleaning properties of the PB strain sensor against ordinary liquid foods were also studied. As illustrated in Figure 7D, the food droplets (≈50 μL) including vinegar, honey, orange juice, soy sauce, soy milk, and milk are spherical in shape on the sensor surface, regardless of their color, viscosity, composition, and so forth. Similarly, these food droplets could easily roll off the PB strain sensor surface without leaving a trace. As a result, the good self-cleaning property endowed the PB strain sensor with great prevention toward a variety of liquids.

3.6. Application in Human Bodily Motion Detection.

Here, the PB strain sensor was mounted onto the different parts of the body using a transparent breathable medical tape to demonstrate the feasibility of the sensor as a wearable strain sensor. As shown in Figure 8A, the sensor could precisely detect the bending of the finger (from 0° to 90°), realizing the real-time detection of the index finger movement. Besides, the water droplets also had no impact on the sensing property because of the superhydrophobicity of the PB strain sensor, endowing it to be applicable under wet or rainy conditions. In addition, it was also valid for the real-time monitoring of elbow joint movement with a significant resistance variation and excellent reproductivity (Figure 8B). As for the detection of the human bodily motion with a small strain, the PB strain sensor was attached onto the wrist hand to detect the pulse of an adult (Figure 8C). It clearly displayed 10 periodic pulse shapes in 8.2 s, which is fully consistent with the pulse frequency (73 beats min^{-1}) of an healthy adult. Then, the sensor was also assembled onto the throat, and stable and repeatable signals were recorded when the tester drank water (Figure 8D). As a result, the PB-based strain sensor exhibited a

DOI: 10.1021/acsami.9b03421
ACS Appl. Mater. Interfaces 2019, 11, 21904−21914

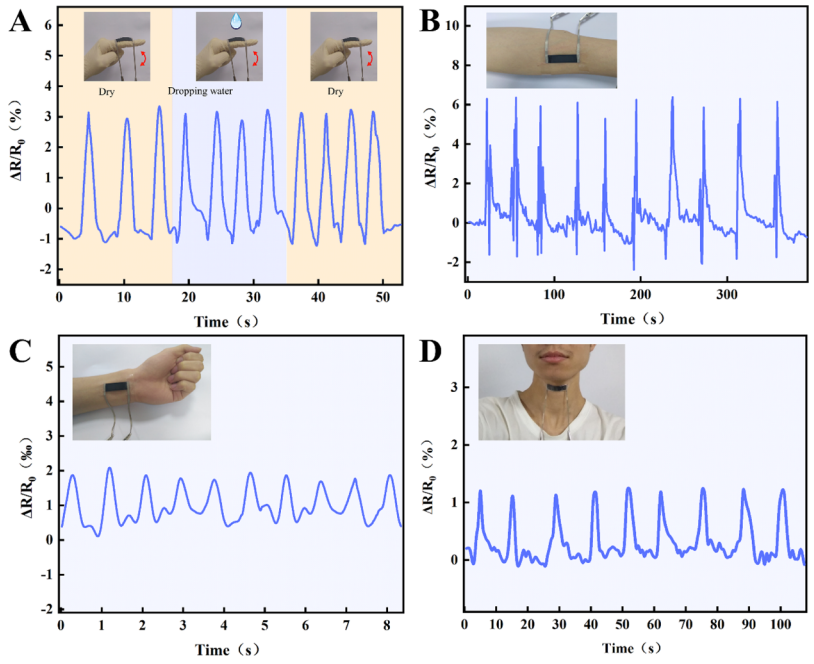

Figure 8. (A) Relative resistance as a function of time about monitoring index finger. Insets: The repetitive bending of the index finger wearing the PB strain sensor under discontinuous water dropping. Real-time variation of the relative resistance when the PB strain sensor was applied to monitor (B) elbow joint movement, (C) wrist pulse, and (D) drinking water.

great potential to detect human bodily motion (especially for the slight motion) for human healthcare application.

4. CONCLUSIONS

In summary, superhydrophobic electrically conductive paper was successfully fabricated by dip-coating the printing paper into an electrically conductive CB/CNT/MC suspension and hydrophobic Hf-SiO_2 suspension successively. A stable aqueous suspension of the conductive filler was achieved with the assistance of the synergistic effect between different dimensional conductive fillers. On the basis of the micro−nano structure and low surface energy of the Hf-SiO_2 layer, the Hf-SiO_2/CB/CNT-coated paper possessed superhydrophobicity with a WCA up to 154°. Meanwhile, lots of microcracks were observed on the CB/CNT layer because of the mismatches of the coating and the substrate material in the thermal expansion coefficient and the elastic modulus during the drying process. In a strain sensor, the closure and propagation of microcracks upon compression and tension led to the decrease and increase of resistance, and their corresponding GFs were calculated to be 2.6 and 7.5 during the strain range of 0−0.7%, respectively. Notably, the PB strain sensor also exhibited an ultralow detection limit of 0.1%. During the cyclic tension process, the PB strain sensor displayed stable, reproducible, durable, and frequency-independent strain sensing behavior. In addition, the superhydrophobicity of the sensor was also well-maintained even after 1000 tension cycles, and the PB strain sensor possessed excellent anticorrosion and self-cleaning properties. Finally, the superhydrophobic PB strain sensor can be used to detect human bodily motion and physiological signals for human healthcare, especially for the wet or rainy conditions.

■ ASSOCIATED CONTENT

Supporting Information

The Supporting Information is available free of charge on the ACS Publications website at DOI: 10.1021/acsami.9b03421.

Composition of CB/CNT and MC in mixed solvent (DI water/ethanol = 1/1); comparison of the properties of the superhydrophobic strain sensor in the references and that in our work; universal testing machine and digital multimeter coupled to record the data of resistance during the bending process; digital photos of CB/MWCNT suspension in 6 h after sonication; energy-dispersive X-ray spectrum of the surface of the Hf-SiO_2/CB/CNT-coated paper; FT-IR spectra of Hf-SiO_2 and the Hf-SiO_2/CB/CNT-coated paper; current−voltage (I−V) curves of the sensor under original, tension, and released state after 1000 times cyclic tension at a strain of 0.6% (PDF)

Hf-SiO_2/CB/CNT-coated paper displaying a strong light reflection when immersed in water (AVI)

Dust particles attached on the surface of the sensor taken away immediately by water droplets during the water-flushing process (AVI)

■ AUTHOR INFORMATION

Corresponding Author

*E-mail: liuhu@zzu.edu.cn.

ORCID

Qianming Li: 0000-0002-7965-2698
Hu Liu: 0000-0003-3840-8135
Xianhu Liu: 0000-0002-4975-3586
Liwei Mi: 0000-0001-9239-6599
Chuntai Liu: 0000-0001-9751-6270
Zhanhu Guo: 0000-0003-0134-0210

Notes

The authors declare no competing financial interest.

■ ACKNOWLEDGMENTS

The authors gratefully acknowledge the financial support for this work by National Natural Science Foundation of China

DOI: 10.1021/acsami.9b03421
ACS Appl. Mater. Interfaces 2019, 11, 21904−21914

(contract numbers: 51803191, 11572290, 11432003), China Postdoctoral Science Foundation (2018M642782), Postdoctoral Research Grant in Henan Province (001801007), the 111 project (D18023), and the National Key Research and Development Program of China (2016YFB0101602). H.L. appreciates the start-up fund from Zhengzhou University.

REFERENCES

(1) Hu, W.; Lum, G. Z.; Mastrangeli, M.; Sitti, M. Small-Scale Soft-Bodied Robot with Multimodal Locomotion. *Nature* **2018**, *554*, 81.
(2) Lu, H.; Zhang, M.; Yang, Y.; Huang, Q.; Fukuda, T.; Wang, Z.; Shen, Y. A Bioinspired Multilegged Soft Millirobot that Functions in Both Dry and Wet Conditions. *Nat. Commun.* **2018**, *9*, 3944.
(3) Lipomi, D. J.; Vosgueritchian, M.; Tee, B. C.-K.; Hellstrom, S. L.; Lee, J. A.; Fox, C. H.; Bao, Z. Skin-Like Pressure and Strain Sensors Based on Transparent Elastic Films of Carbon Nanotubes. *Nat. Nanotechnol.* **2011**, *6*, 788−792.
(4) Qiao, Y.; Wang, Y.; Tian, H.; Li, M.; Jian, J.; Wei, Y.; Tian, Y.; Wang, D.-Y.; Pang, Y.; Geng, X.; Wang, X.; Zhao, Y.; Wang, H.; Deng, N.; Jian, M.; Zhang, Y.; Liang, R.; Yang, Y.; Ren, T.-L. Multilayer Graphene Epidermal Electronic Skin. *ACS Nano* **2018**, *12*, 8839−8846.
(5) (a) Li, G.; Dai, K.; Ren, M.; Wang, Y.; Zheng, G.; Liu, C.; Shen, C. Aligned Flexible Conductive Fibrous Networks for Highly Sensitive, Ultrastretchable and Wearable Strain Sensors. *J. Mater. Chem. C* **2018**, *6*, 6575−6583. (b) Zhang, S.; Liu, H.; Yang, S.; Shi, X.; Zhang, D.; Shan, C.; Mi, L.; Liu, C.; Shen, C.; Guo, Z. Ultrasensitive and Highly Compressible Piezoresistive Sensor Based on Polyurethane Sponge Coated with a Cracked Cellulose Nanofibril/Silver Nanowire Layer. *ACS Appl. Mater. Interfaces* **2019**, *11*, 10922−10932.
(6) Bhattacharjee, M.; Nemade, H. B.; Bandyopadhyay, D. Nano-enabled paper humidity sensor for mobile based point-of-care lung function monitoring. *Biosens. Bioelectron.* **2017**, *94*, 544−551.
(7) Dutta, S.; Mandal, N.; Bandyopadhyay, D. Paper-based α-amylase detector for point-of-care diagnostics. *Biosens. Bioelectron.* **2016**, *78*, 447−453.
(8) Liu, H.; Huang, W. J.; Gao, J. C.; Dai, K.; Zheng, G. Q.; Liu, C. T.; Shen, C. Y.; Yan, X. R.; Guo, J.; Guo, Z. H. Piezoresistive Behavior of Porous Carbon Nanotube-Thermoplastic Polyurethane Conductive Nanocomposites with Ultrahigh Compressibility. *Appl. Phys. Lett.* **2016**, *108*, 011904.
(9) Huang, W.; Dai, K.; Zhai, Y.; Liu, H.; Zhan, P.; Gao, J.; Zheng, G.; Liu, C.; Shen, C. Flexible and Lightweight Pressure Sensor Based on Carbon Nanotube/Thermoplastic Polyurethane-Aligned Conductive Foam with Superior Compressibility and Stability. *ACS Appl. Mater. Interfaces* **2017**, *9*, 42266−42277.
(10) Wang, M.; Zhang, K.; Dai, X.-X.; Li, Y.; Guo, J.; Liu, H.; Li, G.-H.; Tan, Y.-J.; Zeng, J.-B.; Guo, Z. Enhanced Electrical Conductivity and Piezoresistive Sensing in Multi-Wall Carbon Nanotubes/Polydimethylsiloxane Nanocomposites Via the Construction of a Self-Segregated Structure. *Nanoscale* **2017**, *9*, 11017−11026.
(11) Zheng, Y.; Li, Y.; Li, Z.; Wang, Y.; Dai, K.; Zheng, G.; Liu, C.; Shen, C. The Effect of Filler Dimensionality on the Electromechanical Performance of Polydimethylsiloxane Based Conductive Nanocomposites for Flexible Strain Sensors. *Compos. Sci. Technol.* **2017**, *139*, 64−73.
(12) White, M. S.; Kaltenbrunner, M.; Głowacki, E. D.; Gutnichenko, K.; Kettlgruber, G.; Graz, I.; Aazou, S.; Ulbricht, C.; Egbe, D. A. M.; Miron, M. C.; Major, Z.; Scharber, M. C.; Sekitani, T.; Someya, T.; Bauer, S.; Sariciftci, N. S. Ultrathin, Highly Flexible and Stretchable PLEDs. *Nat. Photonics* **2013**, *7*, 811−816.
(13) Pang, C.; Lee, G.-Y.; Kim, T.-i.; Kim, S. M.; Kim, H. N.; Ahn, S.-H.; Suh, K.-Y. A Flexible and Highly Sensitive Strain-Gauge Sensor Using Reversible Interlocking of Nanofibres. *Nat. Mater.* **2012**, *11*, 795−801.
(14) Lu, Y.; Biswas, M. C.; Guo, Z.; Jeon, J.-W.; Wujcik, E. K. Recent Developments in Bio-Monitoring Via Advanced Polymer Nanocomposite-Based Wearable Strain Sensors. *Biosens. Bioelectron.* **2019**, *123*, 167−177.
(15) Yang, Y.; Gao, W. Wearable and Flexible Electronics for Continuous Molecular Monitoring. *Chem. Soc. Rev.* **2019**, *48*, 1465−1491.
(16) Yin, F.; Yang, J.; Peng, H.; Yuan, W. Flexible and Highly Sensitive Artificial Electronic Skin Based on Graphene/Polyamide Interlocking Fabric. *J. Mater. Chem. C* **2018**, *6*, 6840−6846.
(17) Chen, S.; Wei, Y.; Wei, S.; Lin, Y.; Liu, L. Ultrasensitive Cracking-Assisted Strain Sensors Based on Silver Nanowires/Graphene Hybrid Particles. *ACS Appl. Mater. Interfaces* **2016**, *8*, 25563−25570.
(18) Liu, H.; Dong, M.; Huang, W.; Gao, J.; Dai, K.; Guo, J.; Zheng, G.; Liu, C.; Shen, C.; Guo, Z. Lightweight Conductive Graphene/Thermoplastic Polyurethane Foams with Ultrahigh Compressibility for Piezoresistive Sensing. *J. Mater. Chem. C* **2017**, *5*, 73−83.
(19) Liu, H.; Huang, W.; Yang, X.; Dai, K.; Zheng, G.; Liu, C.; Shen, C.; Yan, X.; Guo, J.; Guo, Z. Organic Vapor Sensing Behaviors of Conductive Thermoplastic Polyurethane-Graphene Nanocomposites. *J. Mater. Chem. C* **2016**, *4*, 4459−4469.
(20) Li, L.; Bai, Y.; Li, L.; Wang, S.; Zhang, T. A Superhydrophobic Smart Coating for Flexible and Wearable Sensing Electronics. *Adv. Mater.* **2017**, *29*, 1702517.
(21) Liu, H.; Li, Q.; Zhang, S.; Yin, R.; Liu, X.; He, Y.; Dai, K.; Shan, C.; Guo, J.; Liu, C.; Shen, C.; Wang, X.; Wang, N.; Wang, Z.; Wei, R.; Guo, Z. Electrically Conductive Polymer Composites for Smart Flexible Strain Sensors: A Critical Review. *J. Mater. Chem. C* **2018**, *6*, 12121−12141.
(22) Zhang, Y.; Zhang, L.; Cui, K.; Ge, S.; Cheng, X.; Yan, M.; Yu, J.; Liu, H. Flexible Electronics Based on Micro/Nanostructured Paper. *Adv. Mater.* **2018**, *30*, 1801588.
(23) Guan, X.; Zheng, G.; Dai, K.; Liu, C.; Yan, X.; Shen, C.; Guo, Z. Carbon Nanotubes-Adsorbed Electrospun PA66 Nanofiber Bundles with Improved Conductivity and Robust Flexibility. *ACS Appl. Mater. Interfaces* **2016**, *8*, 14150−14159.
(24) Yang, P.-K.; Lin, Z.-H.; Pradel, K. C.; Lin, L.; Li, X.; Wen, X.; He, J.-H.; Wang, Z. L. Paper-Based Origami Triboelectric Nanogenerators and Self-Powered Pressure Sensors. *ACS Nano* **2015**, *9*, 901−907.
(25) Boehle, K. E.; Gilliland, J.; Wheeldon, C. R.; Holder, A.; Adkins, J. A.; Geiss, B. J.; Ryan, E. P.; Henry, C. S. Utilizing Paper-Based Devices for Antimicrobial-Resistant Bacteria Detection. *Angew. Chem., Int. Ed. Engl.* **2017**, *56*, 6886−6890.
(26) (a) Tan, M. J.; Owh, C.; Chee, P. L.; Kyaw, A. K. K.; Kai, D.; Loh, X. J. Biodegradable Electronics: Cornerstone for Sustainable Electronics and Transient Applications. *J. Mater. Chem. C* **2016**, *4*, 5531−5558. (b) Singh, A. K.; Mandal, T. K.; Bandyopadhyay, D. Magnetically Guided Chemical Locomotion of Self-Propelling Paperbots. *RSC Adv.* **2015**, *5*, 64444−64449.
(27) liu, H.; Jiang, H.; Du, F.; Zhang, D.; Li, Z.; Zhou, H. Flexible and Degradable Paper-Based Strain Sensor with Low Cost. *ACS Sustain. Chem. Eng.* **2017**, *5*, 10538−10543.
(28) Liao, X.; Zhang, Z.; Liao, Q.; Liang, Q.; Ou, Y.; Xu, M.; Li, M.; Zhang, G.; Zhang, Y. Flexible and Printable Paper-Based Strain Sensors for Wearable and Large-Area Green Electronics. *Nanoscale* **2016**, *8*, 13025−13032.
(29) Dong, X.; Wei, Y.; Chen, S.; Lin, Y.; Liu, L.; Li, J. A Linear and Large-Range Pressure Sensor Based on A Graphene/Silver Nanowires Nanobiocomposites Network and a Hierarchical Structural Sponge. *Compos. Sci. Technol.* **2018**, *155*, 108−116.
(30) Ma, Z.; Wei, A.; Ma, J.; Shao, L.; Jiang, H.; Dong, D.; Ji, Z.; Wang, Q.; Kang, S. Lightweight, Compressible and Electrically Conductive Polyurethane Sponges Coated with Synergistic Multi-walled Carbon Nanotubes and Graphene for Piezoresistive Sensors. *Nanoscale* **2018**, *10*, 7116−7126.
(31) Wu, X.; Han, Y.; Zhang, X.; Zhou, Z.; Lu, C. Large-Area Compliant, Low-Cost, and Versatile Pressure-Sensing Platform Based on Microcrack-Designed Carbon Black@Polyurethane Sponge for

DOI: 10.1021/acsami.9b03421
ACS Appl. Mater. Interfaces 2019, 11, 21904−21914

Human-Machine Interfacing. *Adv. Funct. Mater.* **2016**, *26*, 6246−6256.
(32) Yazdani, H.; Hatami, K.; Khosravi, E.; Harper, K.; Grady, B. P. Strain-Sensitive Conductivity of Carbon Black-Filled PVC Composites Subjected to Cyclic Loading. *Carbon* **2014**, *79*, 393−405.
(33) Middya, S.; Bhattacharjee, M.; Mandal, N.; Bandyopadhyay, D. RGO-Paper Sensor for Point-of-Care Detection of Lipase in Blood Serum. *IEEE Sens. Lett.* **2018**, *2*, 1−4.
(34) Liu, H.; Li, Y.; Dai, K.; Zheng, G.; Liu, C.; Shen, C.; Yan, X.; Guo, J.; Guo, Z. Electrically Conductive Thermoplastic Elastomer Nanocomposites at Ultralow Graphene Loading Levels for Strain Sensor Applications. *J. Mater. Chem. C* **2016**, *4*, 157−166.
(35) Zeng, Z.; Liu, M.; Xu, H.; Liao, Y.; Duan, F.; Zhou, L.-m.; Jin, H.; Zhang, Z.; Su, Z. Ultra-Broadband Frequency Responsive Sensor Based on Lightweight and Flexible Carbon Nanostructured Polymeric Nanocomposites. *Carbon* **2017**, *121*, 490−501.
(36) Gao, J.; Wang, X.; Zhai, W.; Liu, H.; Zheng, G.; Dai, K.; Mi, L.; Liu, C.; Shen, C. Ultrastretchable Multilayered Fiber with a Hollow-Monolith Structure for High-Performance Strain Sensor. *ACS Appl. Mater. Interfaces* **2018**, *10*, 34592−34603.
(37) Gao, X.; Zhang, S.; Mai, F.; Lin, L.; Deng, Y.; Deng, H.; Fu, Q. Preparation of High Performance Conductive Polymer Fibres from Double Percolated Structure. *J. Mater. Chem.* **2011**, *21*, 6401−6408.
(38) Liu, X.; Li, C.; Pan, Y.; Schubert, D. W.; Liu, C. Shear-Induced Rheological and Electrical Properties of Molten Poly(Methyl Methacrylate)/Carbon Black Nanocomposites. *Composites, Part B* **2019**, *164*, 37−44.
(39) Pan, Y.; Liu, X.; Kaschta, J.; Hao, X.; Liu, C.; Schubert, D. W. Viscoelastic and Electrical Behavior of Poly(Methyl Methacrylate)/Carbon Black Composites Prior to and After Annealing. *Polymer* **2017**, *113*, 34−38.
(40) (a) Mandal, N.; Bhattacharjee, M.; Chattopadhyay, A.; Bandyopadhyay, D. Point-of-care-testing of α-amylase activity in human blood serum. *Biosens. Bioelectron.* **2019**, *124−125*, 75−81. (b) Bhattacharjee, M.; Bandyopadhyay, D. Mechanisms of Humidity Sensing on A Cds Nanoparticle Coated Paper Sensor. *Sens. Actuators, A* **2019**, *285*, 241−247.
(41) Lu, L.; Wei, X.; Zhang, Y.; Zheng, G.; Dai, K.; Liu, C.; Shen, C. A flexible and self-formed sandwich structure strain sensor based on AgNW decorated electrospun fibrous mats with excellent sensing capability and good oxidation inhibition properties. *J. Mater. Chem. C* **2017**, *5*, 7035−7042.
(42) Lin, L.; Deng, H.; Gao, X.; Zhang, S.; Bilotti, E.; Peijs, T.; Fu, Q. Modified resistivity-strain behavior through the incorporation of metallic particles in conductive polymer composite fibers containing carbon nanotubes. *Polym. Int.* **2013**, *62*, 134−140.
(43) Wei, Y.; Chen, S.; Li, F.; Lin, Y.; Zhang, Y.; Liu, L. Highly Stable and Sensitive Paper-Based Bending Sensor Using Silver Nanowires/Layered Double Hydroxides Hybrids. *ACS Appl. Mater. Interfaces* **2015**, *7*, 14182−14191.
(44) Liu, H.; Gao, J.; Huang, W.; Dai, K.; Zheng, G.; Liu, C.; Shen, C.; Yan, X.; Guo, J.; Guo, Z. Electrically Conductive Strain Sensing Polyurethane Nanocomposites with Synergistic Carbon Nanotubes and Graphene Bifillers. *Nanoscale* **2016**, *8*, 12977−12989.
(45) Lee, S.; Shin, S.; Lee, S.; Seo, J.; Lee, J.; Son, S.; Cho, H. J.; Algadi, H.; Al-Sayari, S.; Kim, D. E.; Lee, T. Ag Nanowire Reinforced Highly Stretchable Conductive Fibers for Wearable Electronics. *Adv. Funct. Mater.* **2015**, *25*, 3114−3121.
(46) Zhao, W.; Kong, J.; Liu, H.; Zhuang, Q.; Gu, J.; Guo, Z. Ultrahigh Thermally Conductive and Rapid Heat Responsive Poly(Benzobisoxazole) Nanocomposites with Self-Aligned Graphene. *Nanoscale* **2016**, *8*, 19984−19993.
(47) Lin, L.; Liu, S.; Zhang, Q.; Li, X.; Ji, M.; Deng, H.; Fu, Q. Towards Tunable Sensitivity of Electrical Property to Strain for Conductive Polymer Composites Based on Thermoplastic Elastomer. *ACS Appl. Mater. Interfaces* **2013**, *5*, 5815−5824.
(48) Zhao, J.; Dai, K.; Liu, C.; Zheng, G.; Wang, B.; Liu, C.; Chen, J.; Shen, C. A Comparison Between Strain Sensing Behaviors of Carbon Black/Polypropylene and Carbon Nanotubes/Polypropylene Electrically Conductive Composites. *Composites, Part A* **2013**, *48*, 129−136.
(49) Wu, X.; Lu, C.; Zhang, X.; Zhou, Z. Conductive Natural Rubber/Carbon Black Nanocomposites Via Cellulose Nanowhisker Templated Assembly: Tailored Hierarchical Structure Leading to Synergistic Property Enhancements. *J. Mater. Chem. A* **2015**, *3*, 13317−13323.
(50) Wei, Y.; Chen, S.; Dong, X.; Lin, Y.; Liu, L. Flexible piezoresistive sensors based on "dynamic bridging effect" of silver nanowires toward graphene. *Carbon* **2017**, *113*, 395−403.
(51) Zhao, H.; Bai, J. Highly Sensitive Piezo-Resistive Graphite Nanoplatelet-Carbon Nanotube Hybrids/Polydimethylsilicone Composites with Improved Conductive Network Construction. *ACS Appl. Mater. Interfaces* **2015**, *7*, 9652−9659.
(52) Ke, K.; Pötschke, P.; Wiegand, N.; Krause, B.; Voit, B. Tuning the Network Structure in Poly(vinylidene fluoride)/Carbon Nanotube Nanocomposites Using Carbon Black: Toward Improvements of Conductivity and Piezoresistive Sensitivity. *ACS Appl. Mater. Interfaces* **2016**, *8*, 14190−14199.
(53) Deng, H.; Ji, M.; Yan, D.; Fu, S.; Duan, L.; Zhang, M.; Fu, Q. Towards tunable resistivity-strain behavior through construction of oriented and selectively distributed conductive networks in conductive polymer composites. *J. Mater. Chem. A* **2014**, *2*, 10048−10058.
(54) Zhou, Y.; Zhou, Y.; Deng, H.; Fu, Q. A Novel Route Towards Tunable Piezoresistive Behavior in Conductive Polymer Composites: Addition of Insulating Filler with Different Size and Surface Characteristics. *Composites, Part A* **2017**, *96*, 99−109.
(55) Deng, H.; Lin, L.; Ji, M.; Zhang, S.; Yang, M.; Fu, Q. Progress on the Morphological Control of Conductive Network in Conductive Polymer Composites and the Use As Electroactive Multifunctional Materials. *Prog. Polym. Sci.* **2014**, *39*, 627−655.
(56) Xu, W.; Lu, Z.; Sun, X.; Jiang, L.; Duan, X. Superwetting Electrodes for Gas-Involving Electrocatalysis. *Acc. Chem. Res.* **2018**, *51*, 1590−1598.
(57) Ding, G.; Jiao, W.; Chen, L.; Yan, M.; Hao, L.; Wang, R. A Self-Sensing, Superhydrophobic, Heterogeneous Graphene Network with Controllable Adhesion Behavior. *J. Mater. Chem. A* **2018**, *6*, 16992−17000.
(58) Si, Y.; Guo, Z. Superhydrophobic Nanocoatings: From Materials to Fabrications and to Applications. *Nanoscale* **2015**, *7*, 5922−5946.
(59) Su, X.; Li, H.; Lai, X.; Chen, Z.; Zeng, X. Highly Stretchable and Conductive Superhydrophobic Coating for Flexible Electronics. *ACS Appl. Mater. Interfaces* **2018**, *10*, 10587−10597.
(60) Wang, P.; Sun, B.; Liang, Y.; Han, H.; Fan, X.; Wang, W.; Yang, Z. A Stretchable and Super-Robust Graphene Superhydrophobic Composite for Electromechanical Sensor Application. *J. Mater. Chem. A* **2018**, *6*, 10404−10410.
(61) Zhang, D.; Cheng, Z.; Kang, H.; Yu, J.; Liu, Y.; Jiang, L. A Smart Superwetting Surface with Responsivity in Both Surface Chemistry and Microstructure. *Angew. Chem., Int. Ed. Engl.* **2018**, *57*, 3701−3705.
(62) Su, B.; Tian, Y.; Jiang, L. Bioinspired Interfaces with Superwettability: From Materials to Chemistry. *J. Am. Chem. Soc.* **2016**, *138*, 1727.
(63) Yang, T.; Li, X.; Jiang, X.; Lin, S.; Lao, J.; Shi, J.; Zhen, Z.; Li, Z.; Zhu, H. Structural Engineering of Gold Thin Films with Channel Cracks for Ultrasensitive Strain Sensing. *Mater. Horiz.* **2016**, *3*, 248−255.
(64) Lee, J.; Kim, S.; Lee, J.; Yang, D.; Park, B. C.; Ryu, S.; Park, I. A Stretchable Strain Sensor Based on a Metal Nanoparticle Thin Film for Human Motion Detection. *Nanoscale* **2014**, *6*, 11932−11939.
(65) Kang, D.; Pikhitsa, P. V.; Choi, Y. W.; Lee, C.; Shin, S. S.; Piao, L.; Park, B.; Suh, K.-Y.; Kim, T.-i.; Choi, M. Ultrasensitive Mechanical Crack-Based Sensor Inspired by the Spider Sensory System. *Nature* **2014**, *516*, 222−226.
(66) Cai, G.; Yang, M.; Pan, J.; Cheng, D.; Xia, Z.; Wang, X.; Tang, B. Large-Scale Production of Highly Stretchable CNT/Cotton/

DOI: 10.1021/acsami.9b03421
ACS Appl. Mater. Interfaces 2019, 11, 21904−21914

Spandex Composite Yarn for Wearable Applications. *ACS Appl. Mater. Interfaces* **2018**, *10*, 32726−32735.
(67) Liu, M.; Wang, S.; Jiang, L. Nature-Inspired Superwettability Systems. *Nat. Rev. Mater.* **2017**, *2*, 17036.
(68) Liao, X.; Liao, Q.; Yan, X.; Liang, Q.; Si, H.; Li, M.; Wu, H.; Cao, S.; Zhang, Y. Flexible and Highly Sensitive Strain Sensors Fabricated by Pencil Drawn for Wearable Monitor. *Adv. Funct. Mater.* **2015**, *25*, 2395−2401.
(69) (a) Gong, S.; Schwalb, W.; Wang, Y.; Chen, Y.; Tang, Y.; Si, J.; Shirinzadeh, B.; Cheng, W. A Wearable and Highly Sensitive Pressure Sensor with Ultrathin Gold Nanowires. *Nat. Commun.* **2014**, *5*, 3132. (b) Trung, T. Q.; Tien, N. T.; Kim, D.; Jang, M.; Yoon, O. J.; Lee, N.-E. A Flexible Reduced Graphene Oxide Field-Effect Transistor for Ultrasensitive Strain Sensing. *Adv. Funct. Mater.* **2014**, *24*, 117−124.

DOI: 10.1021/acsami.9b03421
ACS Appl. Mater. Interfaces 2019, 11, 21904−21914